LO-phonon-assisted cyclotron resonance in a special asymmetric hyperbolic-type quantum well

Khang D. Pham [a], Le Dinh [b], Pham T. Vinh [b, d], C.A. Duque [c], Huynh V. Phuc [d, *], Chuong V. Nguyen [e, **]

[a] *Institute of Research and Development, Duy Tan University, Da Nang, 550000, Viet Nam*
[b] *Physics Department, College of Education, Hue University, Hue, 530000, Viet Nam*
[c] *Grupo de Materia Condensada-UdeA, Instituto de Física, Facultad de Ciencias Exactas y Naturales, Universidad de Antioquia UdeA, Calle 70 No. 52-21, Medellín, Colombia*
[d] *Division of Theoretical Physics, Dong Thap University, Dong Thap, 870000, Viet Nam*
[e] *Department of Materials Science and Engineering, Le Quy Don Technical University, Ha Noi 100000, Viet Nam*

ARTICLE INFO

ABSTRACT

This paper is devoted to the study of the phonon-assisted cyclotron resonance (PACR) in a special asymmetric hyperbolic-type (SAsH) quantum well, in which the two-photon absorption process and the electron−LO-phonon interaction have been included. The PACR effect has been investigated through considering the magneto-optical absorption coefficient (MOAC) and the full-width at half maximum (FWHM). Our results showed that it is better to investigate MOAC and FWHM when the *a*-parameter value of the quantum well is in the range from 9.72 nm to 37.14 nm. The threshold energy decreases non-linearly with the *a*-parameter but increases linearly with the magnetic field. The resonant peaks caused by the emission phonon process are observed significantly. MOAC gives red-shift with the increase of *a*-parameter, gives blue-shift with the rise of magnetic field, but unchanged with the change of temperature, while MOAC's intensities increase with the increase of these three parameters. FWHM decreases with the rise of *a*-parameter but increases with the growth of temperature and magnetic field in both the emission and absorption phonon processes.

1. Introduction

Cyclotron resonance effect has been demonstrated to be one of the useful techniques to directly measure the information about material's characteristics such as the Fermi surface cross-section, the electron effective mass, and the longitudinal-optical (LO) phonon energy [1−3]. Especially, cyclotron resonance is proved to be dominant in measuring the difference between energy levels in solids when an external magnetic field is applied [4]. The absorbed photon energy, $\hbar\Omega$, at which the absorption process happens could be determined by the condition $\hbar\Omega = p\hbar\omega_B$, where p is an integer and $\hbar\omega_B$ is the energy of the Landau spacing (or re-called cyclotron energy in the present study). However, in the dipole approximation, because of the selection rules the absorption at the other values of the energies, which are not

satisfied the above condition, is not allowed. This prohibition could be lifted if the electron-LO-phonon interaction is included [5]. This means that the selection rule is modified to be $\hbar\Omega = p\hbar\omega_B \pm \hbar\omega_0$ with $\hbar\omega_0$ being LO-phonon energy. In this case, the effect is known as the LO-phonon-assisted cyclotron resonance (PACR), which is the main issue of this study.

The PACR was first studied theoretically by Bass and Lenvinson [6] and then by Enck et al. [7]. After that, this effect was observed experimentally for the first time in InSb by McCombe et al. [8]. After these pioneering works, PACR effect has attracted the considerable interest of many researchers because of its great uses. Using Kubo formula, Singh and Tanatar have driven the optical absorption coefficient through the conductivity tensor in a *p*-type [9] as well as in an *n*-type [10] quantum wells. Their results showed that besides the usual cyclotron resonance peak, there was an extra peak in the optical absorption spectrum due to PACR transitions. Using Pidgeon-Brown energy-band model [11], Goodwin and Seiler [12] have succeeded in unifying and explaining the experimental results on the intra-conduction-band magneto-optical in *n*-type InSb. Besides, in this work, they have also presented their own new experimental result on PACR harmonics. The literature of experimental investigations of PACR has also been added by the work of Morita et al. [13], where the unaccustomed dependence of the peak shift, the full-width at half-maximum (FWHM), and the peak intensity of PACR on the magnetic field has been observed. Bhat et al. have studied the PACR due to the scattering between an electron and confined LO-phonons, the interface phonon [14] and confined-acoustic phonons [15] in square quantum wells. Using the perturbation method, the authors predicted a series of extra peaks due to PACR besides the usual cyclotron resonance peak. Despite its simplicity, the method has been demonstrated to be useful in analyzing PACR in quantum wells. However, one disadvantage of the method is that it has only allowed dealing with the one-photon process, while the two-photon ones is still opened.

In a previous work [16], we presented a technique for studying PACR effect in the two-dimensional quantum well using the perturbation approach, in which the two-photon process was included. After that, the technique has been applied successfully to analyse the PACR in quantum wells [17], in quantum well-wires [18], and in graphene [19,20]. Following these works, we have kept developing the technique and have introduced a new version of the optical absorption coefficient in the two-dimensional systems when a magnetic field is applied, renamed MOAC, in which the electron-photon interaction part of the transition matrix element has been improved [21]. One benefit of this technique is that it is simpler than the others methods, such as Kubo theory [22−25] or projection technique [26−28]. In this work, we will apply this technique to analyse the theory of PACR in a special asymmetric hyperbolic-type (SAsH) quantum well. Our calculations predicted PACR peaks caused by the two-photon process besides the one-photon ones. Also, we performed numerical calculations to illustrate the effect of the quantum well parameters, the applied magnetic field, and the temperature on the MOAC and the FWHM when the electron−LO-phonon interaction is involved.

2. The characteristics of the SAsH quantum well model

We consider a SAsH quantum well in which the confining potential in the *z*-direction is given as follows [29,30].

$$U(z) = U_0 \left(\frac{a}{z} - \frac{z}{a} \right)^2, \tag{1}$$

where U_0 is the confinement potential height and a is a quantum well parameter, which has the unit of length. The quantum well shape for three values of the *a*-parameter is illustrated in Fig. 1. We can see that the bigger value of the *a*-parameter is the more asymmetric quantum well shape is.

When a static magnetic field is applied to the *z*-direction of the system ($\mathbf{B} = (0,0,B)$), the Hamiltonian of a single electron in SAsH quantum well reads
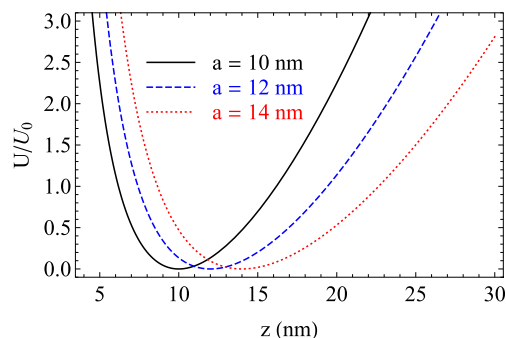

Fig. 1. Quantum well shape for different values of *a*-parameter.

$$\mathscr{H} = \frac{1}{2m^*}(\mathbf{p} + e\mathbf{A})^2 + U(z),$$ (2)

where $\mathbf{p}$ is the momentum operator, e is the absolute value of electron charge, $\mathbf{A} = (0, Bx, 0)$ is the vector potential closely associated with the magnetic field, and $m^* = 0.067m_0$ [31] is the electron effective mass with m_0 being the free electron mass. The electron eigenfunctions and eigenvalues associated with the Hamiltonian (2) are [14,15].

$$\left|\lambda\right\rangle = \left|n, m, k_y\right\rangle = \frac{e^{ik_y y}}{\sqrt{L_y}}\psi_n(x - x_0)\xi_m(z),$$ (3)

$$E_\alpha \equiv E_{n,m} = \left(n + \frac{1}{2}\right)\hbar\omega_B + \varepsilon_m, \ n = 0, 1, 2, \dots.$$ (4)

Here, the integer n stands for the Landau level index, $\psi_n(x - x_0)$ refers to the normalized harmonic-oscillator function centered at $x_0 = -\alpha_B^2 k_y$ with $\alpha_B = (\hbar/m^*\omega_B)^{1/2}$ being the magnetic length which is closely associated with the cyclotron frequency, $\omega_B = eB/m^*$; k_y and L_y respectively being the y-direction electron wave vector and normalization length. The component eigenfunctions and eigenvalues in z-direction are given by Refs. [29,30].

$$\xi_m(z) = C_m z^{\alpha+1/2}e^{-\beta z^2}\,_1F_1\left(-m, \alpha + 1, 2\beta z^2\right),$$ (5)

$$\varepsilon_m = \frac{2\hbar}{a}\sqrt{\frac{2U_0}{m^*}}\left(m + \frac{1}{2} + \frac{\alpha}{2} - a^2\beta\right), \ m = 0, 1, 2, \dots,$$ (6)

where $\beta = (m^*U_0/2\hbar^2 a^2)^{1/2}$ having the unit of m^{-2}, $\alpha = (16a^4\beta^2 + 1)^{1/2}/2$ being a dimensionless quantity, and $_1F_1$ refers to the confluent hypergeometric functions. The normalization constants C_m for the two first states are given as follows: $C_0 = 2^{\alpha/2+1}\beta^{(\alpha+1)/2}/(\Gamma(\alpha+1))^{1/2}$ and $C_1 = C_0(\alpha+1)^{1/2}$. For the further calculations the below useful matrix elements are needed

$$\langle\lambda|x|\lambda'\rangle = \left[x_0\delta_{n',n} + \left(\alpha_B\big/\sqrt{2}\right)\left(\sqrt{n}\,\delta_{n',n-1} + \sqrt{n+1}\,\delta_{n',n+1}\right)\right]\delta_{kk'},$$ (7)

$$\mathscr{F}_{mm'}(\pm q_z) = \int_0^\infty e^{\pm iq_z z}\xi_m^*(z)\xi_{m'}(z)dz,$$ (8)

where $\delta_{kk'} = \delta_{mm'}\delta_{k_{y'},k_y}$.

3. LO-phonon-assisted cyclotron resonance

We now proceed to study the PACR in the SAsH quantum well model. To do this, we need to derive the expression of the MOAC, which can be performed using the perturbative theory developed and applied successfully in Ref. [21]. Taking into account the electron−phonon scattering, the expression for MOAC in the two-dimensional systems, due to absorbing photons of energy $\hbar\Omega$, is given as follows

$$K(\hbar\Omega) = \frac{1}{V_0(I/\hbar\Omega)}\sum_{\lambda,\lambda'}\mathscr{W}_{\lambda,\lambda'}^{\pm}f_\lambda\left(1 - f_{\lambda'}\right).$$ (9)

Here, we use the parameters as they appeared in Ref. [21], i.e., V_0 is the system volume, I is the optical intensity, $\mathscr{W}_{\lambda,\lambda'}^{\pm}$ is the transition matrix element per unit area, and $f_\lambda = f_{n,m} = [e^{(E_{m,n}-E_F)/(k_BT)} + 1]^{-1}$ is Fermi distribution function for λ-state with E_F being the Fermi energy level and k_B being the Boltzmann constant.

From Eq. (8) the overlap integral for the transition between the two lowest states is found to be

$$J_{01} = \int_{-\infty}^{+\infty}|\mathscr{F}_{01}(\pm q_z)|^2 dq_z.$$ (10)

In general, the integral over q_z in Eq. (10) cannot be done analytically. However, according to the suggestion from Gol'dman et al. [29], for the case of $U_0 = 228$ meV and $a = \frac{9.72}{37.14}$ nm (which would be used for the numerical calculations in Sec. 4), the quantity $16a^4\beta^2$ will be much bigger than 1. Thus, we have the relation $\alpha/2 - a^2\beta \approx 0$, and the energy spectrum in Eq. (6) will be read

$$\varepsilon_m = \frac{2\hbar}{a}\sqrt{\frac{2U_0}{m^*}}\left(m + \frac{1}{2}\right),\tag{11}$$

which is the same as energy of an oscillator with a frequency of $\omega_z = (8U_0/m^*a^2)^{1/2}$. In the light of this approximation, the integral in Eq. (10) becomes possible, and the result is

$$J_{01} = \frac{\sqrt{\pi}}{2}\left(\frac{2m^*U_0}{\hbar^2 a^2}\right)^{1/4}.\tag{12}$$

Using the eigenfunctions presented in Eq. (3) and the method given in Ref. [21], we find the following expression for the MOAC in SAsH quantum well, in the case of $m = 0, m' = 1$ and including the two-photon absorption process

$$K(\hbar\Omega) = A(\hbar\Omega)\sum_{n,n'}|\mathcal{B}_{\lambda\lambda'}|^2 J_{01} f_{n,0}\left(1 - f_{n',1}\right)\left\{N_0^-\delta\left(M_1^-\right) + N_0^+\delta\left(M_1^+\right)\right.$$

$$\left. + \frac{\alpha_0^2}{8\alpha_B^2}(n + n' + 1)\left[N_0^-\delta\left(M_2^-\right) + N_0^+\delta\left(M_2^+\right)\right]\right\}\tag{13}$$

where we have denoted $\mathcal{B}_{\lambda\lambda'} = \langle\lambda|x|\lambda'\rangle$ which is presented in Eq. (7), and

$$A(\hbar\Omega) = \frac{S^2 e^4 \alpha_0^2 \chi^* \hbar\omega_0}{32\pi^2 n_r c\varepsilon_0^2 V_0 \alpha_C^6 \hbar^2\Omega},\tag{14}$$

$$M_\ell^\pm = \Delta E \pm \hbar\omega_0 - \ell\hbar\Omega, \quad \ell = 1, 2.\tag{15}$$

Here, S is the area of the sample, $\chi^* = (1/\chi_\infty - 1/\chi_0)$ with $\chi_\infty = 10.89$ and $\chi_0 = 13.18$ [31], α_0 refers to the dressing parameter, n_r is the refractive index of the material, c is the speed of light in vacuum, ε_0 is the permittivity of vacuum, $\Delta E = E_{n',1} - E_{n,0}$ is the threshold energy, and $N_0^\pm = N_0 + 1/2 \pm 1/2$ with $N_0 = [e^{\hbar\omega_0/(k_BT)} - 1]^{-1}$ being Bose distribution of LO-phonon of energy $\hbar\omega_0 = 36.25$ meV [31]. The plus (minus) sign stands for the emission (absorption) process of one phonon.

Finally, the delta functions in Eq. (3) will be handled by changing them by the Lorentzians of width $\gamma^\pm$, i.e., $\delta(M_\ell^\pm) = (\gamma^\pm/\pi)[(M_\ell^\pm)^2 + (\gamma^\pm)^2]^{-1}$, where

$$(\gamma^\pm)^2 = \frac{e^2\chi^* V_0 \hbar\omega_0}{16\pi^{3/2}\varepsilon_0 pS\alpha_c}\sqrt[4]{\frac{2m^*U_0}{\hbar^2 a^2}}N_0^\pm,\tag{16}$$

which is derived from Eq. (A6) of Ref. [22].

4. Numerical results and discussion

We will now discuss the PACR effect in such GaAs SAsH quantum well through investigating the MOAC and FWHM, in which we only consider the transition between two first states, i.e., the transition from the $|0, 0, 0\rangle$-state to $|1, 1, 0\rangle$ ones. We use the following characteristics in our numerical calculations: the electron density $n_e = 3 \times 10^{16}$ cm^{-3} corresponding to the Fermi energy of $E_F = 84.57$ meV. The other parameters are $n_r = 3.2$, $\alpha_0 = 7.5$ nm, and $U_0 = 228$ meV [31–33].

From Eq. (13) we can see that the intensity (or value) of the MOAC depends strongly on the product $f_{n,0}(1 - f_{n',1})$. Therefore, it is necessary to show the dependence of this product on the important parameters such as a-parameter and temperature, and this product for the case of for $n = 0, n' = 1$ is illustrated in Fig. 2. In spite of the significant role in the high-temperature region of the electron-LO-phonon interaction, we want to state here the effect of temperature on the product in the extensive range of temperature, even down to near 0 K. When $T \to 0$ K, all contours tend to converge at $a_1 = 9.72$ nm and $a_2 = 37.14$ nm. At these two special values of the a-parameter, the ground and the first excited energy levels equal to Fermi energy level, respectively. Moreover, when the value of a-parameter is in the interval from a_1 to a_2, the value of the product $f_{0,0}(1 - f_{1,1})$ is greater than that in the other ranges. Therefore, it is better to study MOAC and FWHM when the a-parameter value is in the range from a_1 to a_2. Besides, when the temperature increases, the Fermi distribution functions $f_{n,0}$ and $f_{n',1}$ will be thermally spread, resulting in the reduction of the product $f_{0,0}(1 - f_{1,1})$.
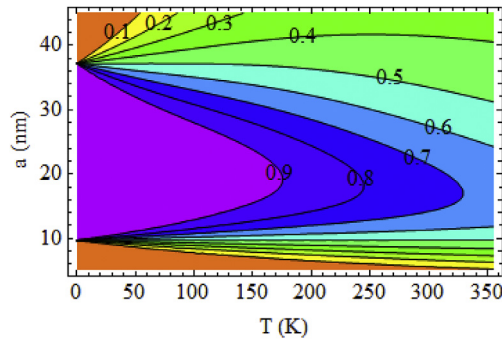
Fig. 2. Contour plot of the product $f_{0,0}(1 - f_{1,1})$ as functions of a-parameter and temperature T at $B = 10$ T.

Besides the product $f_{0,0}(1 - f_{1,1})$, the threshold energy is also one of the essential characteristics affecting the MOAC, especially the resonant peak positions. In Fig. 3, the threshold energy, ΔE, is shown as versus magnetic field for different values of a-parameter. The major feature is that ΔE enhances linearly with the magnetic field but decreases non-linearly with the a-parameter. The features in Figs. 2 and 3 will be used in the following to explain the variation of the peaks values as well as the shifting behavior of the resonant peak positions.

In Fig. 4, MOAC is plotted as functions of photon energy for three different values of a-parameter, the values of $B = 10$ T and $T = 77$ K are chosen for convenient reason in comparing with the other published works [16,17,34]. The four maxima appeared in each curve of Fig. 3, labeled by the numerals from "1″ to "4″ for the solid curve, for example, result from the resonant transitions, which satisfy the conditions

$$\ell\hbar\Omega = \Delta E \pm \hbar\omega_0. \tag{17}$$

In Eq. (17), $\ell = 1$ and 2 stand for the ℓ-photon process. The plus (minus) sign refers to the emission (absorption) process of one LO-phonon. For the physical meaning, these peaks describe the resonant transitions of electrons between the two first
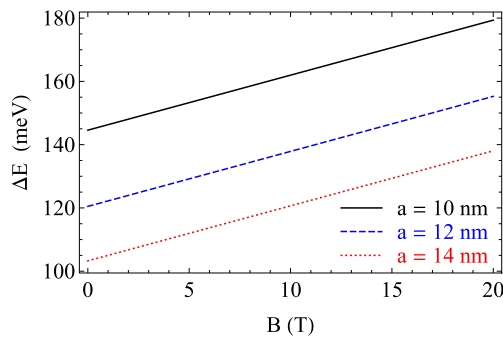

Fig. 3. Threshold energy, $\Delta E = E_{1,1} - E_{0,0}$, versus magnetic field with $a = 10$ nm, 12 nm, and 14 nm, respectively.
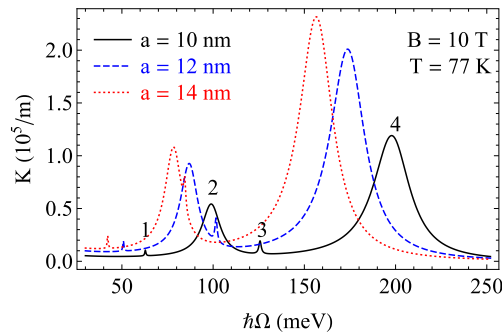

Fig. 4. MOAC versus photon energy, $\hbar\Omega$, for different values of a-parameter.

states due to absorbing one or two photons accompanied with the absorption (peaks "1″ and "3″) or emission (peaks "2″ and "4″) of one LO-phonon. It is worth to note here that unlike in the other types of quantum wells [16,17,34], in SAsH quantum well the resonant peaks due to the phonon emission process are observed significantly.

Another important feature is that for the fixed values of B and T, when the a-parameter increases the resonant peaks give a shift towards the low energy region (red-shift) and the corresponding intensities become bigger. These results are well matched with previous work reported for the third-harmonic generation susceptibility [30]. It is noted that in the above mentioned work, Guang-Hui et al. dealt with smaller values of the a-parameter (a = 1.5, 1.8, and 2 nm), which are much smaller than a_1 mentioned in the discussion part of Fig. 2. In this work, the chosen values of a-parameter are a = 10, 12 and 14 nm to ensure that they are in the range from a_1 to a_2. The red-shift of resonant peaks, observed in Fig. 4, is caused by the reduction of threshold energy with the increase of a-parameter (see Fig. 3). Physically, when the a-parameter is greater, the quantum confining effect will reduce, leading to the narrower energy separation $\Delta\varepsilon_{01} = \varepsilon_1 - \varepsilon_0$, and so does the threshold energy ΔE.

Besides, from Fig. 4 we also see that the peaks intensities due to the phonon absorption process (peaks "1″ and "3″) are much smaller than that due to the emission ones (peaks "2″ and "4″). This is the result of the fact that the LO-phonon population N_0 is much smaller than 1 at the fixed values of B and T.

In Fig. 5, the FWHM is shown as functions of the a-parameter for both the one- (solid symbols) and two-photon (hollow symbols) processes as well as for both the emission and absorption processes of LO-phonon. Since the FWHM has a close relationship with the electron-phonon scattering, the nonlinear decrease of the FWHM with the increase of a-parameter reveals that the electron−LO-phonon scattering in SAsH quantum well decreases when the a-parameter increases. Besides, similar to the peaks intensities shown in Fig. 4, because the LO-phonon population N_0 is much smaller than 1, the FWHM due to phonon emission process (left vertical axis) is also much more significant than that due to absorption ones (right vertical axis). For a more visual look, we detail the fitted results of the a-dependent FWHM as follows: FWHM (meV) $= \beta_1 + \beta_2 a + \beta_3 a^{-1}$, where β_1, β_2, and β_2 are listed in Table 1 for four lines from top to bottom of Fig. 5.

These fitted results are illustrated by the solid red lines in Fig. 5. Unfortunately, there is no experimental result yet available for this problem to support our study. We expect that this prediction would be serviceable for orienting to experimental research in the future.

In Fig. 6, MOAC is plotted as functions of $\hbar\Omega$ for three different values of the temperature. In general, when T is raised the resonant peaks positions are unchanged, but their intensities are enhanced. These features can be explained by the fact that while the resonant peaks positions are specified by the resonant conditions shown in Eq. (17), the temperature dependent peaks intensities are driven by two terms: the phonon population N_0 and the product $f_{0,0}(1 - f_{1,1})$. The T-independent selection rules lead to the fixed locations of the peaks with the change of temperature. Whereas, the explanation of the increasing peaks intensities is complicated. There is a competition between N_0 and the product $f_{0,0}(1 - f_{1,1})$ when the temperature increases: the product decreases (see Fig. 2) while N_0 increases. The increase of the peaks intensities reveals that the effect of N_0-increasing is dominant. Besides, we also see that the effect of the temperature on the transitions due to phonon absorption process is much stronger than that due to the phonon emission ones. This result is well fitted with that calculated for the parabolic quantum well [35] but to be in contrast to the result obtained in a quantum well with the complicated potential [36].
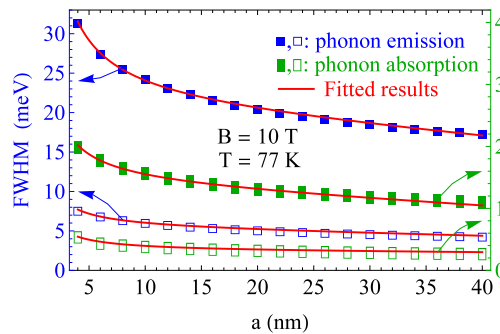

Fig. 5. FWHM versus a-parameter. The solid and hollow symbols respectively indicate the one-photon and two-photon processes.

Table 1
The fitted results of the a-dependent FWHM.

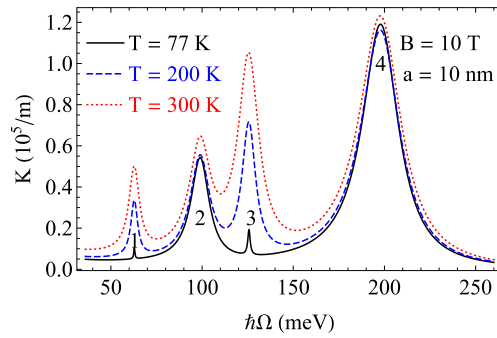| Parameters	Line 1	Line 2	Line 3	Line 4
β_1 (meV)	20.78	1.38	5.34	0.31
β_2 (meV nm^{-1})	− 0.12	− 0.01	− 0.03	− 0.001
β_3 (meV nm)	44.93	2.72	9.98	0.95

Fig. 6. MOAC versus photon energy, $\hbar\Omega$, for different values of temperature.
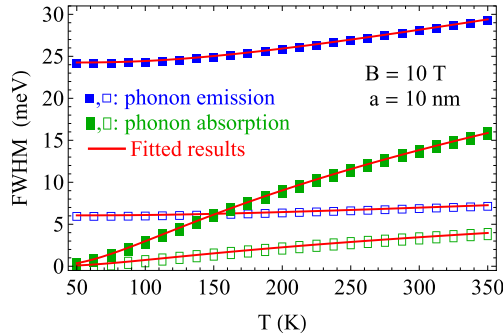

Fig. 7. FWHM versus temperature. The solid and hollow symbols respectively indicate the one-photon and two-photon processes.

Fig. 7 shows the temperature dependence of FWHM for both processes: emission and absorption phonons. The FWHM is seen to rise with the growing temperature in all case: either the one- (solid symbols) or two-photon (hollow symbols) absorption processes as well as both the emission and absorption phonon ones. This expanding behavior of the FWHM can be explained by the thermal broadening resulted from the electron−LO-phonon scattering mechanism. For the phonon emission process, the expression for the dependence of FWHM on temperature can be expressed as follows [37].

$$\text{FWHM (meV)} = a_T + b_T N_0(T), \tag{18}$$

where a_T is the steady part and b_T is the thermal broadening ones of FWHM. With the help of the temperature dependent LO-phonon population function $N_0(T) = [e^{\hbar\omega_0/(k_B T)} - 1]^{-1}$, the best-fit values of a_T and b_T are found to be: $a_T = 24.26$ (6.06) meV and $b_T = 11.92$ (2.81) meV, respectively, for the one- (two-) photon absorption. These fitted results are illustrated by the solid red lines in Fig. 7, which are bigger than those in a quantum well with the complicated potential [36] as well as the experimental reported by Gammon et al. [37].

For the phonon absorption process, instead of Eq. (18) the expression for the *T*-dependent FWHM is now read to be: $\text{FWHM(meV)} = c_T N_0^{1/2}$, where $c_T = 24.18$ for the one- and $c_T = 6.04$ meV for the two-photon processes, respectively.
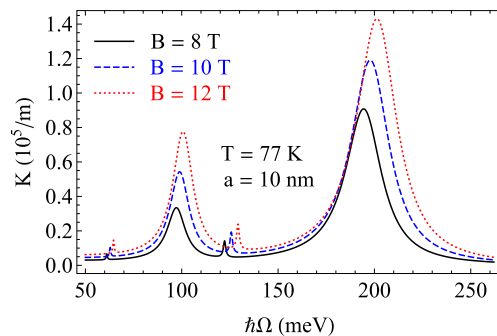

Fig. 8. MOAC versus photon energy for different values of magnetic field.
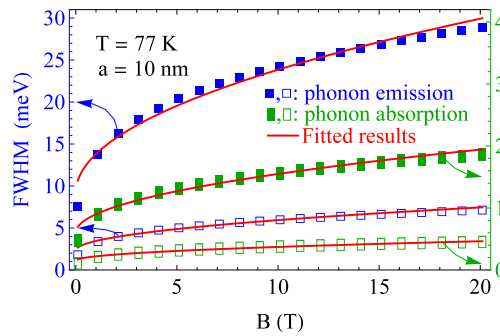
Fig. 9. FWHM versus magnetic field *B*. The solid and hollow symbols respectively indicate the one-photon and two-photon processes.

In Fig. 8, we depict the magnetic field influence on the resonant peaks in SAsH quantum well. We see that the stronger magnetic field is, the higher peaks intensities are, and the more clear blue-shift is. These *B*-dependent features of the resonant peaks are well fitted with those reported in quantum wells [4,14,15,34,36,38,39], in quantum wires [40], in quantum dots [41,42], and in quantum rings [43,44]. The augment of the peaks intensities are resulted from the reduction of the magnetic length α_c with the rise of magnetic field *B*. Meanwhile, the blue-shift feature is the result of the extension of threshold energy with the magnetic field (see Fig. 3). Besides, the increase of magnetic field also leads to the peaks broadening, which is closely related to the enhancement of FWHM as shown in the following.

Fig. 9 displays the influence of magnetic field on the FWHM at fixed values of *a* and *T* for both phonon emission and phonon absorption processes as well as for both one- (solid symbols) and two-photon (hollow symbols) absorption processes. In generally, FWHM displays as a nonlinear increasing function of *B* in all cases. This result fits well with that reported in previous work in bulk materials using the equilibrium density projection technique [27], as well as in other types of quantum wells [36,45], in cylindrical quantum wires [18], and in graphene [28]. To have more accurate results, we show here the analytic expression of the *B*-dependent FWHM as follows: FWHM [meV] $= a_B + b_B(B[\text{T}])^{1/2}$. Here, the best-fit values of a_B and b_B are found to be as follows for the phonon emission process: $a_B = 9.17\ (2.30)$ meV and $b_B = 4.64\ (1.15)$ meV corresponding to the one-photon (two-photon) absorption process. The corresponding values of these parameters for the phonon absorption process are $a_B = 0.60\ (0.15)$ meV and $b_B = 0.30\ (0.07)$ meV. The much bigger of the FWHM in SAsH quantum well in comparison with that in the square quantum well [16] or in a quantum well with the complicated potential [36] reveals that the electron-LO-phonon scattering in SAsH type is stronger than that in the other shapes ones.

5. Conclusion

We have studied in details the PACR in SAsH quantum well via investigating the MOAC and FWHM. The resonant condition is found explicitly. The main conclusion of the present study can be expressed as follows: (i) it is better to study MOAC and FWHM when the *a*-parameter value is in this range from 9.72 nm to 37.14 nm in the case of *B* = 10 T. (ii) The threshold energy decreases non-linearly with the *a*-parameter but increases linearly with the magnetic field. (iii) The resonant peaks due to the emission phonon process are observed significantly in the particular SAsH quantum well model. (iv) The MOAC gives red-shift with the increase of *a*-parameter, blue-shift with the growth of magnetic field, but unchanged with the change of temperature. Meanwhile, MOAC's intensity increases with the rise of these three parameters. (v) The FWHM decreases with the increase of *a*-parameter but increases with the growth of temperature and magnetic field.

Moreover, our results also show that electron-LO-phonon interaction in SAsH quantum well is stronger than that in the other shapes ones. The present result of the thermal broadening FWHM fits well with the previous experiment report. We hope that this result may have a significant contribution to the literature investigations of PACR and the magneto-optical transport properties of such low-dimensional systems. Unfortunately, there is no experimental result yet available for this problem to support our study. We expect that this prediction would be serviceable for orienting to experimental research in the future.

Acknowledgments

References

[1] E.J. Johnson, D.H. Dickey, Phys. Rev. B 1 (1970) 2676.
[2] K.L. Ngai, E.J. Johnson, Phys. Rev. Lett. 29 (1972) 1607.
[3] M. Weiler, R. Aggarwal, B. Lax, Solid State Commun. 14 (1974) 299.
[4] J.S. Bhat, S.S. Kubakaddi, B.G. Mulimani, J. Appl. Phys. 70 (1991) 2216.

 [5] V.I. Ivanov-Omskii, L.I. Korovin, E.M. Shereghii, Phys. Status Solidi B 90 (1978) 11.
 [6] F.G. Bass, I.B. Levinson, Sov. Phys. JETP 22 (1966) 635.
 [7] R.C. Enck, A.S. Saleh, H.Y. Fan, Phys. Rev. 182 (1969) 790.
 [8] B.D. McCombe, S.G. Bishop, R. Kaplan, Phys. Rev. Lett. 18 (1967) 748.
 [9] M. Singh, B. Tanatar, Phys. Rev. B 41 (1990) 12781.
[10] B. Tanatar, M. Singh, Phys. Rev. B 42 (1990) 3077.
[11] C.R. Pidgeon, S.H. Groves, Phys. Rev. 186 (1969) 824.
[12] M.W. Goodwin, D.G. Seiler, Phys. Rev. B 27 (1983) 3451.
[13] S. Morita, S. Takano, H. Kawamura, J. Phys. Soc. Jpn. 39 (1975) 1040.
[14] J.S. Bhat, B.G. Mulimani, S.S. Kubakaddi, Phys. Rev. B 49 (1994) 16459.
[15] J.S. Bhat, R.A. Nesargi, B.G. Mulimani, Phys. Rev. B 73 (2006) 235351.
[16] H.V. Phuc, L. Dinh, T.C. Phong, Superlattice. Microst. 59 (2013) 77.
[17] H.V. Phuc, N.T.T. Thao, L. Dinh, T.C. Phong, J. Phys. Chem. Solid. 75 (2014) 300.
[18] H.V. Phuc, L.T.M. Hue, L. Dinh, T.C. Phong, Superlattice. Microst. 60 (2013) 508.
[19] H.V. Phuc, N.N. Hieu, Optic Commun. 344 (2015) 12.
[20] H.V. Phuc, L. Dinh, Mater. Chem. Phys. 163 (2015) 116.
[21] C.V. Nguyen, N.N. Hieu, N.A. Poklonski, V.V. Ilyasov, L. Dinh, T.C. Phong, L.V. Tung, H.V. Phuc, Phys. Rev. B 96 (2017) 125411.
[22] M.P. Chaubey, C.M. Van Vliet, Phys. Rev. B 33 (1986) 5617.
[23] P. Vasilopoulos, Phys. Rev. B 33 (1986) 8587.
[24] P. Vasilopoulos, M. Charbonneau, C.M. Van Vliet, Phys. Rev. B 35 (1987) 1334.
[25] P. Vasilopoulos, P. Warmenbol, F.M. Peeters, J.T. Devreese, Phys. Rev. B 40 (1989) 1810.
[26] J.Y. Ryu, R.F. O'Connell, Phys. Rev. B 48 (1993) 9126.
[27] J.Y. Sug, S.G. Jo, J. Kim, J.H. Lee, S.D. Choi, Quantum transition processes in deformation potential interacting systems using the equilibrium density projection technique, Phys. Rev. B 64 (2001) 235210.
[28] B.D. Hoi, L.T.T. Phuong, T.C. Phong, J. Appl. Phys. 123 (2018) 094303.
[29] I.I. Gol'dman, V.D. Krivchenkov, V.I. Kogan, V.M. Galitskii, Problems in Quantum Mechanics, Inforsearch, London, 1960.
[30] W. Guang-Hui, G. Kang-Xian, G. Qi, Commun. Theor. Phys. 39 (2003) 377.
[31] S. Adachi, J. Appl. Phys. 58 (1985) R1.
[32] E. Li, Physica E 5 (2000) 215.
[33] F. Ungan, U. Yesilgul, S. Sakiroglu, M.E. Mora-Ramos, C.A. Duque, E. Kasapoglu, H. Sari, I. Sökmen, Optic Commun. 309 (2013) 158.
[34] H.V. Phuc, N.D. Hien, L. Dinh, T.C. Phong, Superlattice. Microst. 94 (2016) 51.
[35] H.V. Phuc, D.Q. Khoa, N.V. Hieu, N.N. Hieu, Optik 127 (2016) 10519.
[36] L.V. Tung, P.T. Vinh, H.V. Phuc, Physica B 539 (2018) 117.
[37] D. Gammon, S. Rudin, T.L. Reinecke, D.S. Katzer, C.S. Kyono, Phys. Rev. B 51 (1995) 16785.
[38] E. Ozturk, I. Sökmen, J. Lumin. 145 (2014) 387.
[39] H. Sari, E. Kasapoglu, S. Sakiroglu, U. Yesilgul, F. Ungan, I. Sökmen, Physica E 90 (2017) 214.
[40] Y. Karaaslan, B. Gisi, S. Sakiroglu, E. Kasapoglu, H. Sari, I. Sökmen, Superlattice. Microst. 93 (2016) 32.
[41] G. Liu, K. Guo, C. Wang, Physica B 407 (2012) 2334.
[42] G. Liu, K. Guo, H. Hassanabadi, L. Lu, Physica B 407 (2012) 3676.
[43] C.M. Duque, A.L. Morales, M.E. Mora-Ramos, C.A. Duque, J. Lumin. 143 (2013) 81.
[44] E.C. Niculescu, D. Bejan, Philos. Mag. A 97 (2017) 2089.
[45] M.P. Chaubey, C.M. Van Vliet, Phys. Rev. B 34 (1986) 3932.